Atmospheric Environment 162 (2017) 55–70

Contents lists available at ScienceDirect

Atmospheric Environment

journal homepage: www.elsevier.com/locate/atmosenv

Spatially and chemically resolved source apportionment analysis: Case study of high particulate matter event

Byeong-Uk Kim [a], Changhan Bae [b], Hyun Cheol Kim [c, d], Eunhye Kim [b], Soontae Kim [b, *]

[a] Georgia Environmental Protection Division, Atlanta, GA 30354, USA
[b] Department of Environmental and Safety Engineering, Ajou University, Suwon 443-749, South Korea
[c] Air Resources Laboratory, National Oceanic and Atmospheric Administration, College Park, MD 20740, USA
[d] Cooperative Institute for Climate and Satellites, University of Maryland, College Park, MD 20740, USA

HIGHLIGHTS

- PM source contributions in Seoul, Korea during late February 2014 were analyzed.
- Domestic contributions grew throughout the episode.
- China and South Korea contributed 70% and 21% of $PM_{2.5}$.
- Major secondary $PM_{2.5}$ components were Chinese SO_4^{2-} and NO_3^- and Korean NH_4^+.
- PM controls for the SMA requires refined strategies in space, time, and chemicals.

GRAPHICAL ABSTRACT

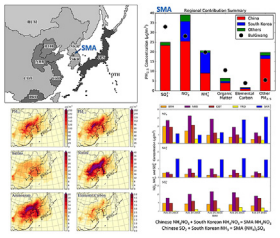

ARTICLE INFO

Article history:
Received 16 February 2017
Received in revised form
27 April 2017
Accepted 3 May 2017
Available online 6 May 2017

Keywords:
Source contribution
Secondary inorganic aerosol
PM event
East Asia
CAMx
South Korea

ABSTRACT

This article presents the results of a detailed source apportionment study of the high particulate matter (PM) event in the Seoul Metropolitan Area (SMA), South Korea, during late February 2014. Using the Comprehensive Air Quality Model with Extensions with its Particulate Source Apportionment Technology (CAMx-PSAT), we defined 10 source regions, including five in China, for spatially and chemically resolved analyses. During the event, the spatially averaged PM_{10} concentration at all PM_{10} monitors in the SMA was 129 $\mu g/m^3$, while the PM_{10} and $PM_{2.5}$ concentrations at the BulGwang Supersite were 143 $\mu g/m^3$ and 123 $\mu g/m^3$, respectively. CAMx-PSAT showed reasonably good PM model performance in both China and the SMA. For February 23–27, CAMx-PSAT estimated that Chinese contributions to the SMA PM_{10} and $PM_{2.5}$ were 84.3 $\mu g/m^3$ and 80.0 $\mu g/m^3$, respectively, or 64% and 70% of the respective totals, while South Korea's respective domestic contributions were 36.5 $\mu g/m^3$ and 23.3 $\mu g/m^3$. We observed that the spatiotemporal pattern of PM constituent concentrations and contributions did not necessarily follow that of total PM_{10} and $PM_{2.5}$ concentrations. For example, Beijing-Tianjin-Hebei produced high nitrate concentrations, but the two most-contributing regions to PM in the SMA were the Near Beijing area and South Korea. In addition, we noticed that the relative contributions from each region changed over time. We found that most ammonium mass that neutralized Chinese sulfate mass in the SMA came from South Korean sources, indicating that secondary inorganic aerosol in the SMA, especially ammonium sulfates, during this event resulted from different major precursors originating from different regions.

* Corresponding author.
E-mail address: soontaekim@ajou.ac.kr (S. Kim).

http://dx.doi.org/10.1016/j.atmosenv.2017.05.006

1. Introduction

Particulate matter (PM) of 10 or 2.5 μm in diameter or less, termed PM_{10} or $PM_{2.5}$, respectively, has raised social policy concerns around the world for decades due to its significant adverse health effects, including premature deaths, identified in numerous studies and references therein (Lipfert, 1994; Vedal, 1997; Kaiser, 1997; Pope and Dockery, 2006; US EPA, 2009; Bell, 2012; Lim et al., 2012; Burnett et al., 2014; Dominici et al., 2014; Héroux et al., 2015). Particulate matter is a complex mixture of directly emitted substances (i.e., primary PM) and products formed chemically (i.e., secondary PM) through atmospheric reactions of their precursors (NARSTO, 2004; Seinfeld and Pandis, 2016). Understanding the causes of PM_{10} and $PM_{2.5}$ air quality problems in an area, therefore, requires assessing the contributions of both local and remote sources while considering the physicochemical processes of PM transport and formation (Stohl et al., 2002; NARSTO, 2004; Chin et al., 2007).

In South Korea, public awareness of serious PM pollution problems has been growing (Kwon et al., 2002; Kim et al., 2007; Chang et al., 2016; Richey and Ohn, 2016). To address these problems, the South Korean government has begun two major efforts. One is the development and operation of the nationwide year-round PM air quality forecast to help public make informed decisions about their outdoor activities since 2012 (Chang et al., 2016). The other is the development and implementation of air quality policies to lower domestic PM levels (Korea Ministry of Environment (2015)). Lowering domestic PM levels is made more difficult by the fact that high PM concentrations observed in South Korea are often linked to emissions from China (National Institute of Environmental Research, 2013; Oh et al., 2015; Shin et al., 2016; Wang et al., 2016). Wherever remote PM sources lie beyond the jurisdictional boundary of the receptor area's authority, as in South Korea, the development of effective control strategies becomes particularly complicated, because addressing air quality problems then requires collaborative efforts (Farrell and Keating, 1998; Dentener et al., 2010; Secretariat of Working Group for LTP project, 2011) This is exactly why the South Korean government has not only implemented local controls (Korea Ministry of Environment, 2015) but has also pursued international collaboration with neighboring countries, such as China and Japan including special campaigns such as ACE-Asia (Han et al., 2004; Seinfeld et al., 2004; Uno et al., 2004; Jung, 2016). Despite these efforts, South Korea still faces challenges in improving the accuracy of its air quality forecasting and in effectively developing a strategy for pollution control. PM is a complex material emitted from both foreign and domestic sources and formed out of precursors from both remote and local sources through atmospheric chemical reactions (NARSTO, 2004; Seinfeld and Pandis, 2016). Thus, improvements to emissions inventories and effective control strategies must account for the geographical origins of both primary PM emissions and precursor emissions for secondary PM.

In this study, we attempted to advance the understanding of the root causes of high PM events in South Korea by analyzing spatially and chemically resolved domestic and foreign source apportionment. As a case study, we conducted detailed source apportionment analyses for the high PM_{10} and $PM_{2.5}$ episode that occurred during late February 2014. This period was one of a few high PM events in 2014 that might not be associated with typical Asian Dust cases (Kim et al., 2016a) and showed the likely dominance of anthropogenic emissions. Over the past two years, several studies have examined this event, each focusing on limited aspects: meteorological characteristics of the event without refined chemical analysis, chemical compositions of observed PM during the event period without spatially specifying emissions sources, chemical analysis without a quantitative assessment of the impact of upwind country emissions on the air quality of downwind areas, or only total mass of PMs without considering PM speciation during the event (Yan et al., 2015; Kim et al., 2016b; Lin et al., 2016; Shin et al., 2016). Therefore, we performed a more comprehensive study of the event to identify the spatial and chemical characteristics of PM, using a photochemical grid model instrumented with a source apportionment tool based on a method of tagging chemical species. This approach can provide spatially specific and chemically resolved source apportionment information. For example, we can quantify how much sulfur dioxide (SO_2) emitted from one foreign source region and nitrogen oxides (NO_X) emitted from another foreign source region contribute to elevated sulfate (SO_4^{2-}) and nitrate (NO_3^-) concentrations observed in the Seoul Metropolitan Area (SMA), South Korea.

The remainder of this article is structured as follows. First, we describe the configuration of the model system, observational data, and overall performance of the modeling system. Next, we discuss the characteristics of foreign and domestic contributions to PM_{10} and $PM_{2.5}$ in the SMA, South Korea with respect to geographical origin and chemical composition. Finally, we identify the cause of high PM events during late February 2014 and propose future studies. Ultimately, we anticipate that the study framework presented here can be generally applicable in analyses on other high PM episodes around the world.

2. Model configuration and observational datasets

2.1. CAMx-PSAT modeling setup

For modeling, we used the Comprehensive Air Quality Model with Extensions (CAMx) with the Particulate Source Apportionment Technology (PSAT) tool (hereafter, CAMx-PSAT). CAMx-PSAT tracks pollutants in a computationally efficient fashion by tagging them based on their origin, including emissions sector and/or geography (Wagstrom et al., 2008; Ramboll-Environ, 2016). CAMx-PSAT tracks primary pollutants directly in the model. For secondary pollutants, it designates certain emitted species as tagged (e.g., SO_2 for sulfate), simulating their physical and chemical changes through the host model's physicochemical solvers. Therefore, CAMx-PSAT does not suffer from the significant non-linear effects that can occur with the brute-force method when large emission perturbations are applied (Yarwood et al., 2007; Wagstrom et al., 2008; Ramboll-Environ, 2016; Qu et al., 2016).

The modeling domains for this study comprise one (27-km) master grid and two (9- and 3-km) nested grids, as shown in Fig. 1. CAMx simulates air movement in these domains simultaneously (i.e., two-way nesting) for each time step to resolve transport and transformation correctly so that it can simulate re circulation between the finer-grid domains and the master grid. This approach can simulate regional transport more accurately than one-way nesting. The ambient air quality monitors, used to evaluate the performance of the modeling system, are marked in Fig. 1. During the chosen study period from February 22 to February 28, 2014, spatially averaged PM_{10} concentrations in the SMA were high, above the daily average 100 $\mu g/m^3$ "high" PM_{10} threshold used by Oh et al. (2015); the following section details the observed data, including that from monitor networks. For source apportionment analysis, 10 source regions were defined in the 27-km master domain, as shown in Fig. 2.

For meteorological model inputs, we used the Weather Research and Forecast (WRF) model (Skamarock and Klemp, 2008) v3.5.1, from which outputs were generated for routine air quality forecasting as part of the Integrated Multi-scale Air Quality System for Korea (IMAQS-K). IMAQS-K also uses various combinations of

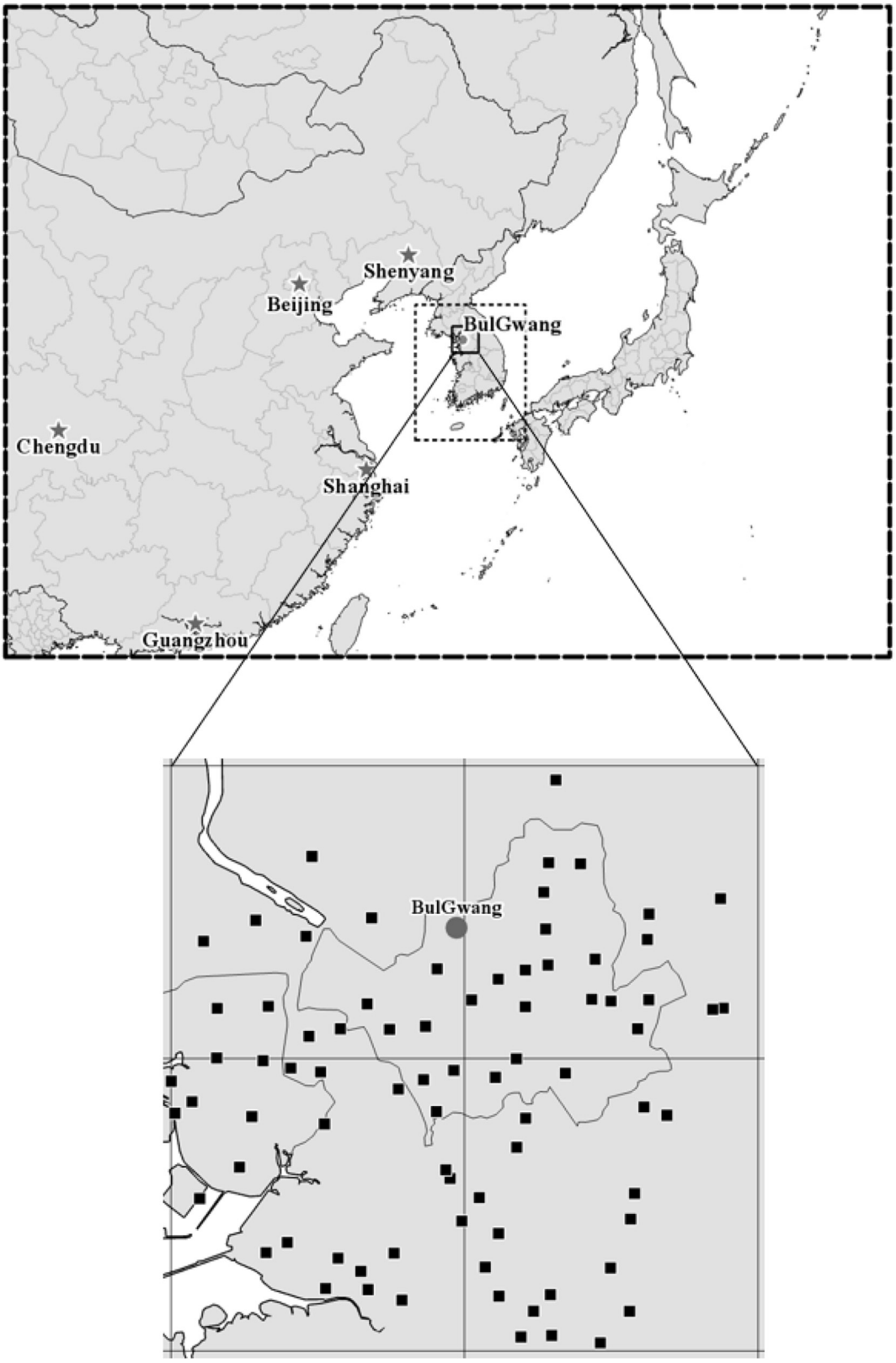

Fig. 1. Modeling domains and monitor locations. The dashed-, dotted-, and solid-line rectangles in the upper panel depict the boundaries of 27, 9, and 3 km grid modeling domains, respectively. Gray stars in the upper panel show the locations of United States Department of State $PM_{2.5}$ monitors. Black squares in the bottom panel depict South Korea's National Institute of Environmental Research PM_{10} monitoring sites. Square boxes with thin black lines in the bottom panel represent four 27-km grid cells. These four cells represent the "SMA" in further analysis. The gray circle in both panels represents the location of the BulGwang Supersite. The Supersite measures total PM_{10} mass concentrations, total $PM_{2.5}$ mass concentrations, and $PM_{2.5}$ species concentrations.

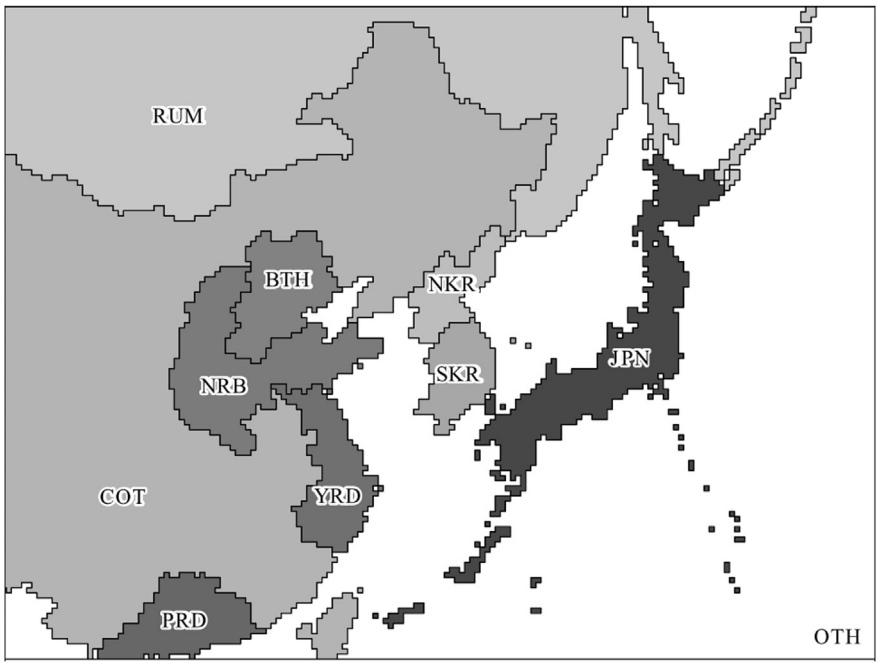

Fig. 2. CAMx-PSAT source regions (and their labels) defined for this study: Beijing-Tianjin-Hebei (BTH), China-Other (COT), North Korea (NKR), Near Beijing (NRB), Japan (JPN), Pearl River Delta (PRD), Russia and Mongolia (RUM), South Korea (SKR), and Yangtze River Delta (YRD). All other areas over the 27-km domain are assigned to the "Others" (OTH) group.

Table 1
Summary of WRF configuration.

Input/Physics	Selected Option
Version	3.5.1
Initial Condition	GFS (1°)
Land use	Korea Ministry of Environment
Number of vertical layers (height of first layer)	30 layers (32 m)
Top of vertical layers	50 hPa
Microphysics	WSM3 (Hong et al., 2004)
Cumulus scheme	Kain-Fritsch (Kain, 2014) for 27- and 9-km domains
Land-Surface Model	NOAH (Chen and Dudhia, 2001)
Planetary Boundary Layer scheme	YSU (Hong et al., 2006)

model-ready inputs processed with Sparse Matrix Operator Kernel Emissions (SMOKE) to perform ensemble forecasting with multiple chemical-transport models. For this study, we utilized IMAQS-K's WRF outputs based on initial conditions and boundary conditions from the Global Forecasting System (GFS) (https://www.ncdc.noaa.gov/data-access/model-data/model-datasets/global-forcast-system-gfs). Table 1 summarizes the configuration of the WRF model. For CAMx model-ready meteorological inputs, we used the WRFCAMx preprocessor. We set the minimum vertical diffusivity to 1.0 m^2/sec for consistency with the current forecasting configuration for IMAQS-K members using the Community Multiscale Air Quality model. Emissions inventories used were the Intercontinental Chemical Transport Experiment-Phase B (INTEX-B) 2006 for foreign anthropogenic emissions (Zhang et al., 2009), the Clean Air Policy Support System (CAPSS) 2007 for domestic anthropogenic emissions (Lee et al., 2011), and the Model of Emissions of Gases and Aerosols from Nature (MEGAN) for biogenic emissions (Guenther, 2006). We used SMOKE to generate model-ready, hourly gridded emissions input files. For the CAMx run, using CAMx v6.1 with the configuration shown in Table 2, we supplied photolysis rate input files prepared with the Tropospheric Visible and Ultraviolet radiation model utility, reflecting outputs of the O3MAP program for adjusting ultraviolet strength based on the Level 3 Ozone Monitoring Instrument product for ozone column data. We used outputs from forecast CAMx runs, which are generated beginning at 3 UTC every day. We excluded the first 12 h of output, taking the next 24 h of data each day for the final analysis.

2.2. Observational data used to evaluate model performance

To evaluate the performance of the meteorological model, we acquired 2-m temperature and 10-m wind speed data at monitors operated by the Korea Meteorological Administration (KMA) in the SMA (Korea Meteorological Administration, 2016). To evaluate performance of the CAMx model, we used observational data from the three monitoring networks shown in Fig. 1: (1) total $PM_{2.5}$ mass concentrations at United States Department of State (USDOS) $PM_{2.5}$ monitors in China (U.S. Department of State, 2016), (2) total PM_{10} mass concentrations at monitors managed by the National Institute of Environmental Research (NIER) in the SMA (Korea Ministry of Environment, 2016), and (3) the BulGwang Supersite operated by the NIER in the SMA (Korea Ministry of Environment, 2016). The "Data Use Statement" from USDOS states that their data are not fully quality-assured. Nevertheless, according to Liang et al. (2016), these US $PM_{2.5}$ monitors show measured values highly consistent with those measured at China's Ministry of Environmental

Table 2
Summary of CAMx configuration.

Physics/Chemistry	Selected Option
Version	6.1
Horizontal Advection	Piece-wise Parabolic Method (Colella and Woodward, 1984)
Gas-phase Chemical Mechanism	SAPRC99 (Carter, 2016)
Aerosol Chemistry	RADM-AQ (Chang et al., 1987) ISORROPIA (Nenes et al., 1998) SOAP (Strader et al., 1999) Static 2-mode (Coarse-Fine; CF Scheme) for size distribution (ENVIRON International Corporation, 2014)
Dry Deposition Model	Resistance model (Zhang et al., 2001; Zhang et al., 2003)
Wet Deposition	Scavenging model (Seinfeld and Pandis, 2016)
PBL Scheme	YSU (Hong et al., 2006)
Minimum Vertical Diffusivity	1.0 m^2/s

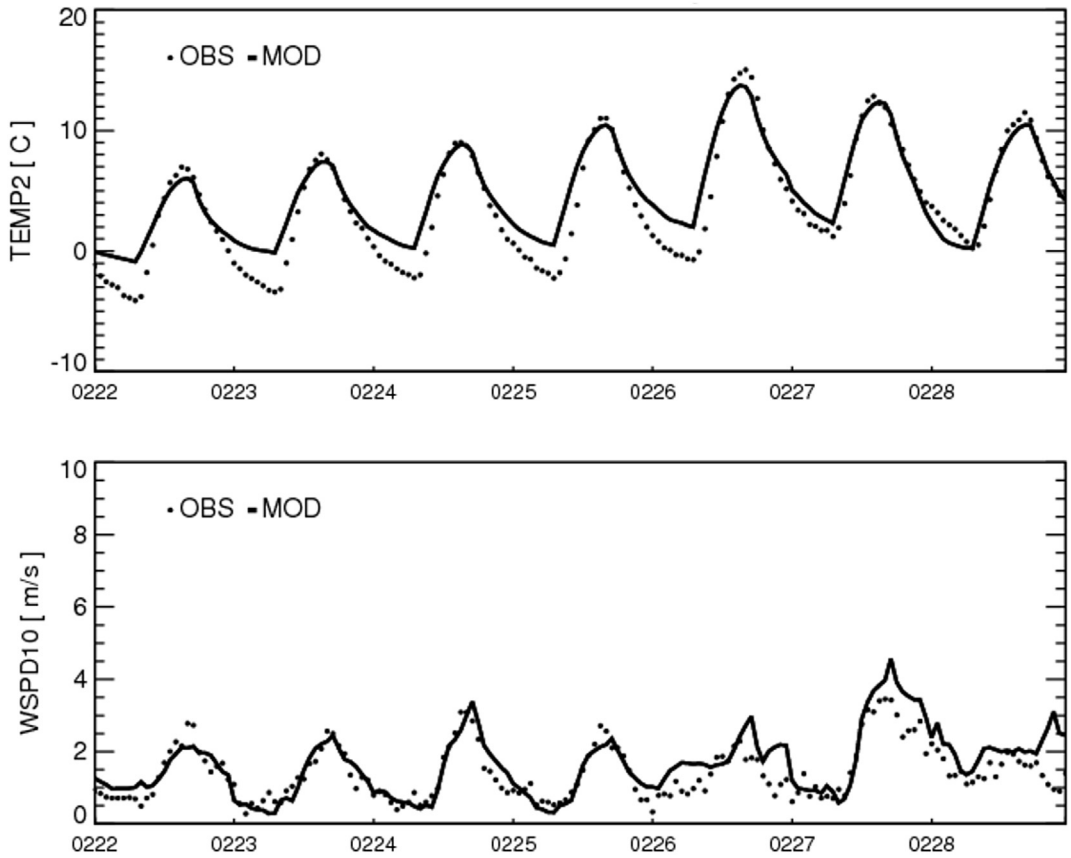

Fig. 3. Spatially averaged time series of hourly observed (dots) and 3-km modeled (solid lines) 2-m temperatures (top) and 10-m wind speeds (bottom) at eight meteorological stations in the SMA. The modeled data outputs in the 3-km domain.

Protection $PM_{2.5}$ monitors located nearby. Thus, we utilized USDOS monitor data to evaluate the performance of the CAMx for $PM_{2.5}$ in China. Since PM_{10} measurements at Chinese monitoring sites are not publicly available, we used $PM_{2.5}$ model performance as a proxy for PM_{10} model performance. While we recognize that this assumption may not be accurate for all high PM_{10} episodes, it can be reasonable for non-Asian Dust events including our study case (Nie et al., 2012; Fu et al., 2014). In the SMA, 81 PM_{10} monitors measured hourly PM_{10} mass concentrations during the case study period. The BulGwang Supersite measured various $PM_{2.5}$ species during the modeled period, including secondary inorganic aerosol components and trace metal elements (Korea Ministry of Environment, 2016; Shin et al., 2016).

3. Results and discussion

3.1. Evaluation of meteorological model performance

To ensure the accuracy of meteorological inputs driving the chemical transport model, we conducted meteorological performance evaluation with time series (Fig. 3) and scatter plots (Fig. S1) comparing observed and modeled 2-m temperature and 10-m wind speeds. The modeled data is output in the 3-km domain. In general, the WRF simulates 2-m temperatures reasonably well. During nighttime, we observed slight over-prediction, though throughout the modeled period the WRF captures diurnal variations, especially rising and falling temperatures, reasonably well. For 10-m wind speeds, the WRF captures daily variations well,

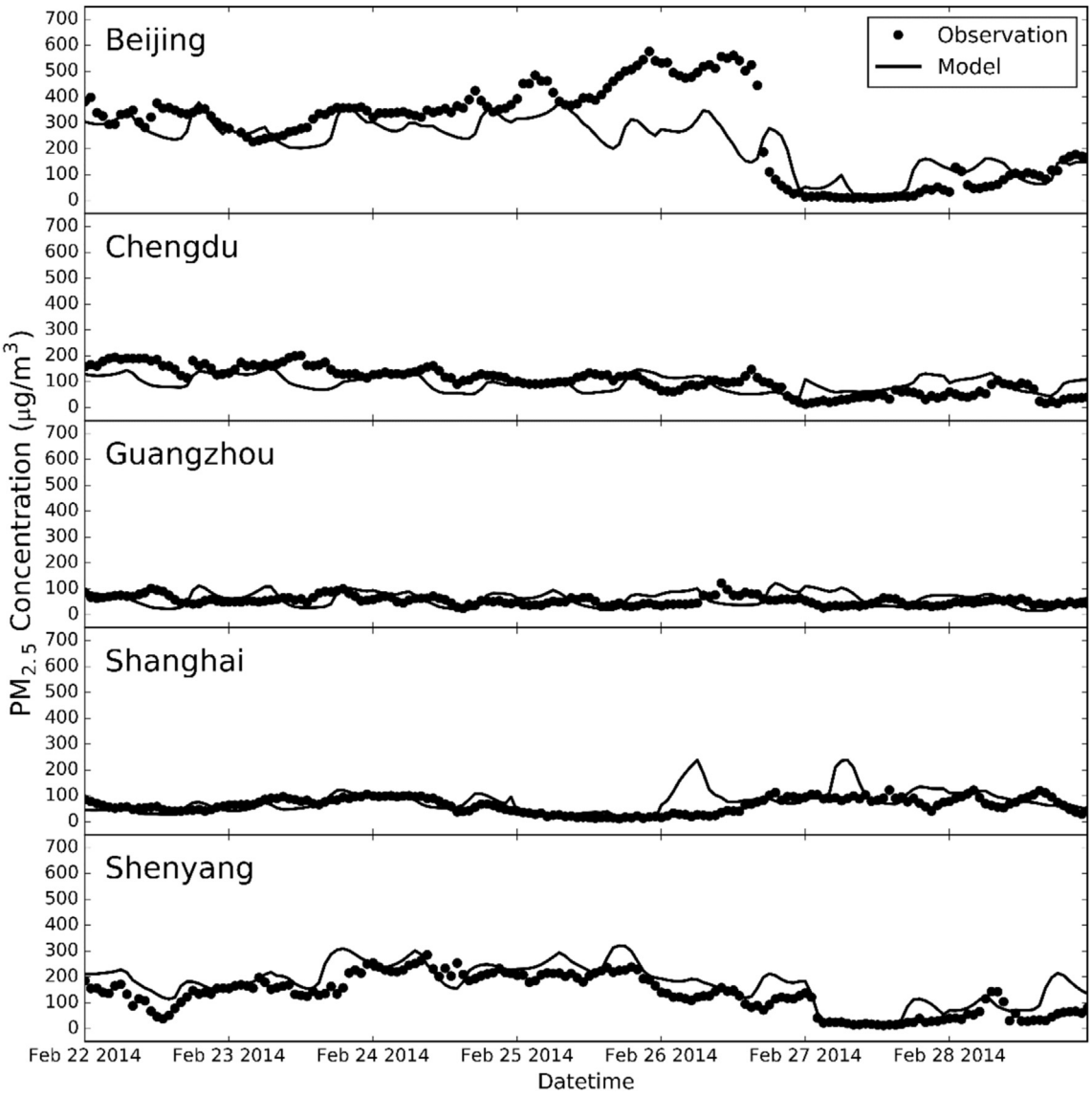

Fig. 4. Time series of observed (dots) and modeled (solid line) $PM_{2.5}$ concentrations at USDOS $PM_{2.5}$ sites in China. The modeled data outputs in the 27-km domain.

except for slight over-prediction on February 26, 27, and 28. However, even on these days, the model still shows a general tendency of wind-speed changes that is reasonably consistent with observation.

3.2. Evaluation of CAMx model performance

Prior to the source apportionment analysis, we examine the model performance of the chemical transport model with time series plots of $PM_{2.5}$ concentrations at USDOS $PM_{2.5}$ sites in China. Overall, CAMx performs reasonably well at all monitor locations, except for under-predictions on February 25 and 26 at the Beijing monitor and slight over-predictions on February 26 and 27 at the Shanghai monitor (Fig. 4). Of all five monitors, Beijing showed the highest $PM_{2.5}$ concentrations throughout the modeling period. The under-prediction observed at the Beijing monitor may lead to potential under-prediction of foreign contributions at the SMA on later dates if air parcels in this area are transported into the SMA in the model. CAMx captures the rapid decrease in $PM_{2.5}$ concentrations starting during the late night of February 27. Overall, we believe CAMx provides great confidence for areas upwind of the SMA, South Korea, which is critical for source-apportionment assessment. Table S1 summarizes the model performance statistics for $PM_{2.5}$ from February 22 to February 27. Nevertheless, further studies are warranted to quantify the impact of model under-/over-prediction at upwind areas on contribution assessments downwind.

Overall, at the hourly level, CAMx agrees well with observations of PM_{10} monitors, except for under-predictions on February 24 and 28 (Fig. 5). In general, the tendency towards under-prediction is larger at the BulGwang Supersite than at the NIER PM_{10} sites, which implies that the BulGwang Supersite may be influenced by local sources or be hit by narrow, transported PM_{10} plumes. Either or both could cause potentially large spatial gradients in the SMA during the modeled period, even though the SMA only covers an area of 54 km by 54 km. Because spatial variation in PM_{10} across the SMA is quite large on some days, we speculate that many monitors in the SMA, including the BulGwang Supersite, are heavily influenced by local, primary PM sources. This possibility of strong local source impacts might not be captured sufficiently in the current

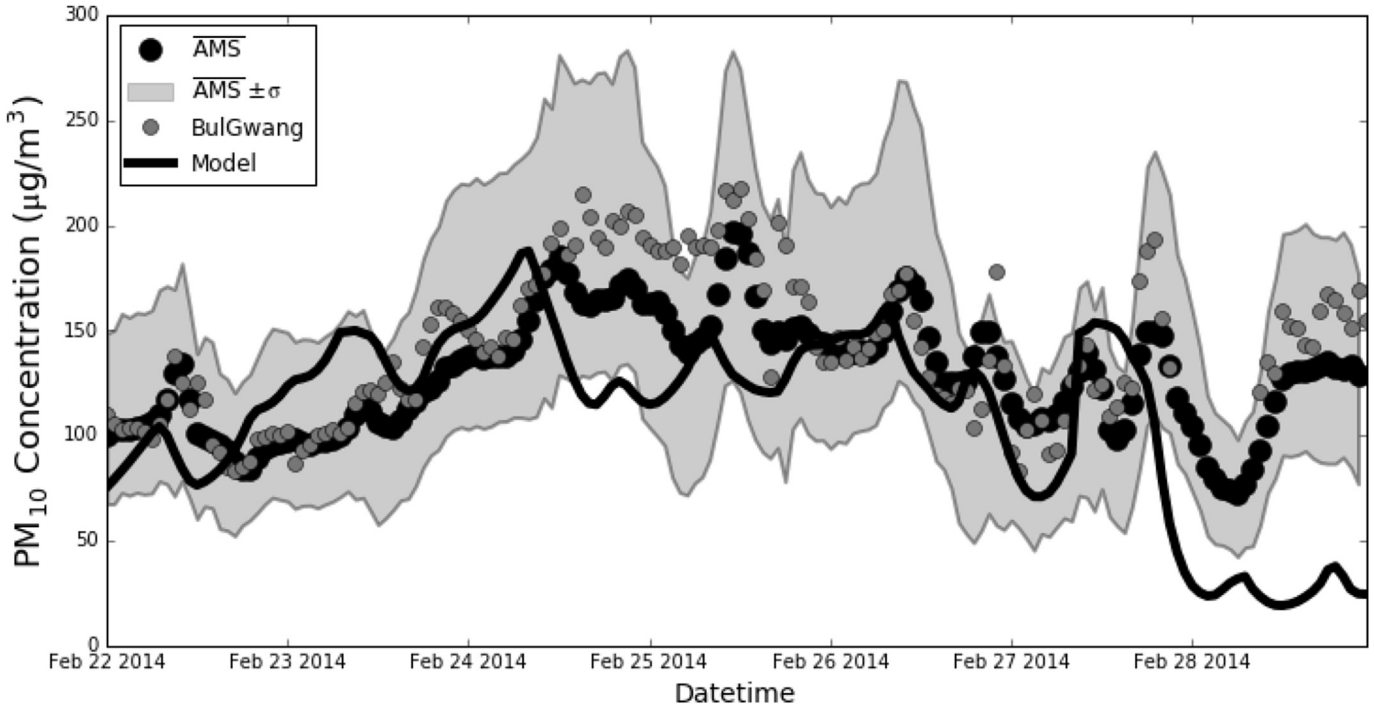

Fig. 5. Time series of observed and modeled PM_{10} concentrations. Circles depict observed concentrations at 81 NIER PM_{10} monitors and at the BulGwang Supersite. The solid line represents modeled PM_{10} concentrations. The NIER data points are average values across all monitors in the SMA, while the modeled data are spatially averaged concentrations over the SMA. Shaded gray areas depict one standard deviation from average PM_{10} concentrations at NIER PM_{10} monitors.

modeling results. Therefore, caution should be taken when source apportionment results are inferred before taking practical actions. At the same time, we examined how airmass arrived at the BulGwang monitor by following the HYSPLIT (Stein et al., 2015) back-trajectory modeling approach used by Han et al. (2004) and Shin et al. (2016). We found that the BulGwang monitor measured quite different airshed compared with the Jeju monitor or even the BaekRyung monitor (Fig.s S2–S4). Nevertheless, further studies are warranted to identify significant local sources that may not be present in the current modeling inventory. The magnitude of under-prediction on February 28 is significant. As examined above for CAMx performance at the USDOS Beijing site, CAMx captures a sudden drop in $PM_{2.5}$ concentrations on February 27 and 28. Further study is necessary to clarify whether the significant under-prediction on February 28 in the SMA is caused by too fast winds or missing emissions in the model near the SMA.

For total $PM_{2.5}$ mass concentrations (Fig. 6), CAMx shows similar tendencies as in the PM_{10} model-observation comparison in Fig. 5. For organic matter, we multiplied measured organic carbon concentrations by 1.6, following Morris et al., (2005b). For "Other $PM_{2.5}$," which is mostly fine crustal, we took the estimation approaches of Malm et al. (1994) and Eldred (2003) to utilize trace-element measurements at the BulGwang Supersite. For details regarding how we derived fine crustal concentrations from the trace-element measurements, we provide a description of our approach in the supplemental material (see Fig. S5). For sulfate, CAMx slightly under-estimates throughout the episode. For nitrate and ammonium, CAMx performs reasonably well although the model noticeably under-predicts from the night of February 22 to the morning of February 24. The model grossly underestimates the concentrations of organic matter. Even using the upper-bound value (1.8) for the mass-adjustment coefficient, as in (Morris et al., 2005b), to estimate aged, that is, very oxygenated organic particles, the under-prediction does not seem to be explained just with additional mass corrections accounting for oxygenated substance due to additional mass corrections accounting for oxygenated substance due to particle aging. CAMx also greatly under-predicts elemental carbon concentrations. Because the modeled episode was in wintertime, we think it unlikely that the organic matter under-prediction is due to the lack of secondary organic aerosols in the model which are produced in large quantities during summertime. Rather, we suspect that most of the under-prediction of organic matter results from shortages in the model of primary organic matter due to the emissions inventory issues. We note that the observed rapid drop of high PM concentrations on February 27 in the Beijing area did not necessarily lead to lowering the PM pollution from the SMA one or two days later. It poses important questions regarding the temporal characteristics of the contributions of domestic and near-source regions, such as NKR. On the other hand, we observed that the model grossly over-predicts other $PM_{2.5}$ concentrations, which are likely more sensitive to local sources than to remote sources. The overall model performance seems reasonably good although we have highlighted areas for improvement.

3.3. Results of PM and source apportionment

To identify the spatial characteristics of modeling results, we examined the average spatial distribution of modeled PM_{10}, $PM_{2.5}$, sulfate, nitrate, ammonium, and elemental carbon concentrations at the model's first layer across the episode. For the purpose of this analysis, we limited our spatial analyses to the period from February 23 to February 27. CAMx simulated concentrations over 200 $\mu g/m^3$ PM_{10} and over 160 $\mu g/m^3$ $PM_{2.5}$ near the Beijing area and spatial distribution patterns of PM_{10} and $PM_{2.5}$ are similar (Fig. 7). We observed very high concentration spots of PM_{10} and $PM_{2.5}$ near Shenyang, with a very steep concentration gradient. Concentration distributions of PM constituents did not necessarily follow the

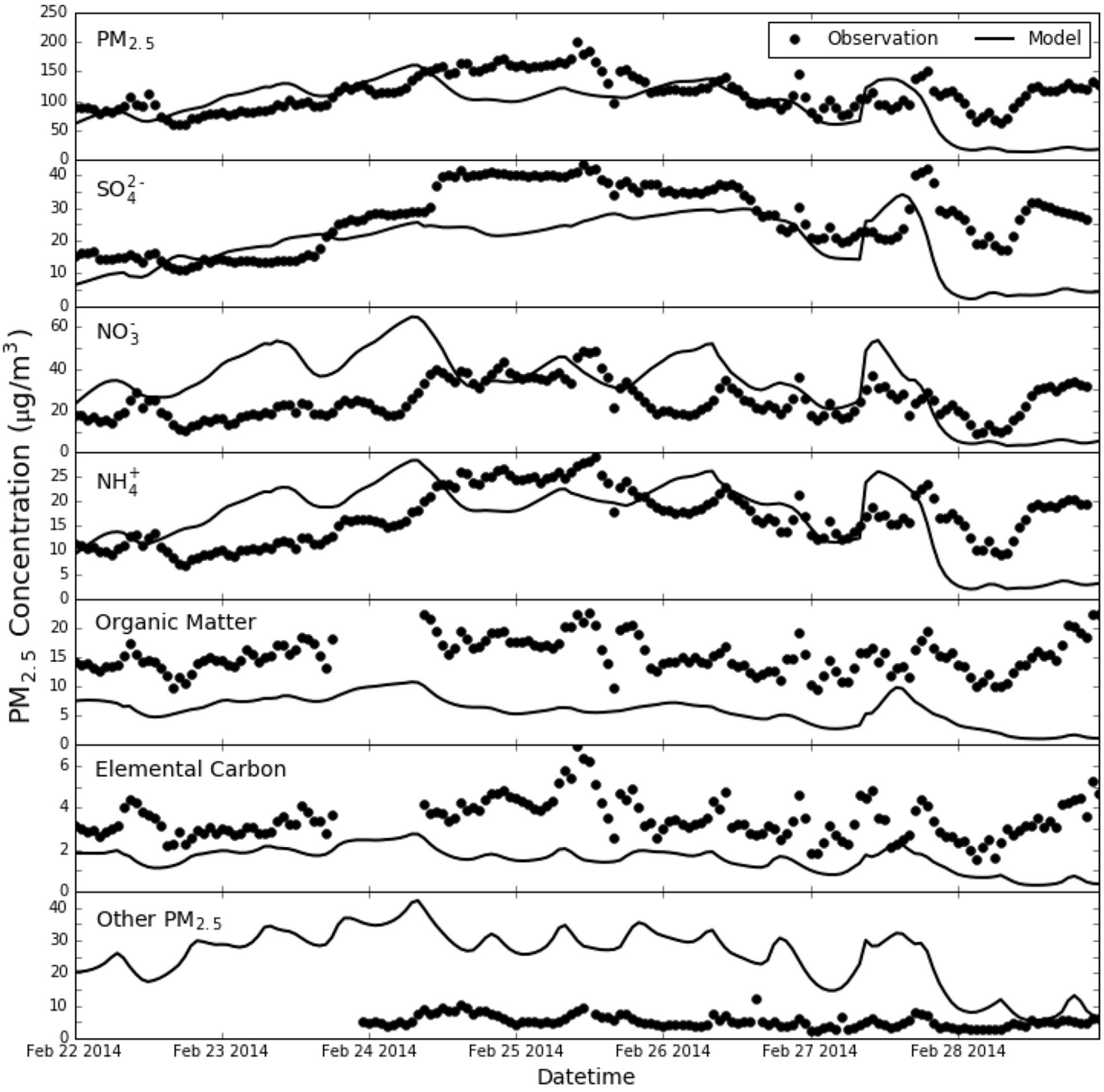

Fig. 6. Time series of observed and modeled $PM_{2.5}$ concentrations. Circles depict observed concentrations at the BulGwang Supersite. The solid line represents modeled $PM_{2.5}$ concentrations, which are spatially averaged concentrations over the SMA.

spatial pattern of total PM_{10} and $PM_{2.5}$ concentration. For example, nitrate concentrations were spread over the area near Beijing, as well as the SMA area. However, high sulfate concentrations appeared over the Yellow Sea, southeast of Beijing (i.e., Tianjin), and the SMA. Overall, CAMx predicted much higher nitrate concentrations than sulfate concentrations in the modeled domain, especially for areas near Beijing and northeastern China. Given the weak photochemistry and low temperatures during wintertime, this modeled result for nitrate agrees with current understanding of its characteristics (Seinfeld and Pandis, 2016). Modeled sulfate, on the other hand, requires further attention; we cannot rule out potential under-estimation of sulfate in China based on the above observation-model comparison at the BulGwang Supersite. Although it is also possible that local SO_2 sources in South Korea might contribute sulfate to the SMA, this was not observed for this episode, as we discuss in greater detail in the following section. Regarding the elemental carbon, the high concentration areas in China are not noticeably different from other major constituents. However, on the Korean peninsula, areas near Pyongyang, North Korea showed relatively high concentrations of elemental carbon. Given that the model at the SMA under-estimated elemental carbon and organic matter concentrations, the possibility of under-estimated primary organic carbons and elemental carbon emissions from combustion processes in North Korea should be

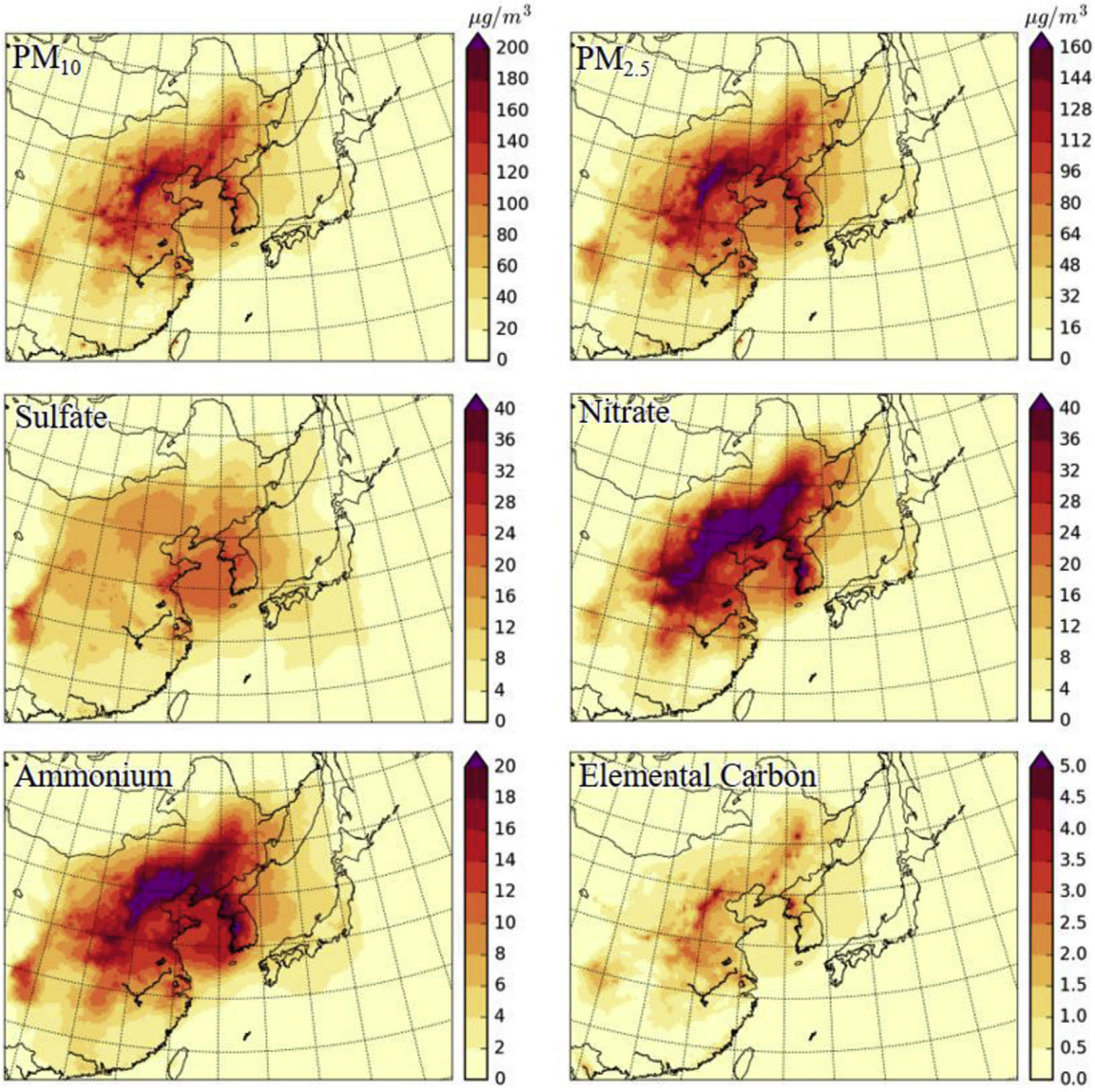

Fig. 7. Spatial distribution of episodic average (February 23 to 27, 2014) concentrations of PM_{10} (top left), $PM_{2.5}$ (top right), sulfate (middle left), nitrate (middle right), ammonium (bottom left), and elemental carbon (bottom right).

investigated to improve the overall model performance at the SMA. Overall, CAMx replicated a characteristic of PM formation in China observed by Gao et al. (2015) for winter haze days not driven by dust storms: a high $PM_{2.5}$-to-PM_{10} ratio and prevalent secondary inorganic aerosols (Tan et al., 2009).

Reviewing average spatial distribution across the episode of modeled nitrate concentrations originating from the four major source regions illustrated in Fig. 2, we noticed that the BTH and COT regions seem to have produced the highest nitrate concentrations in the region during the episode (Fig. 8). However, the two most contributing regions for nitrate concentrations in the SMA appear to have been NRB and SKR, making episodic contributions of 12.1 μg/m^3 and 9.4 μg/m^3, respectively. Among the NRB areas, the eastern Beijing area—Tangshan and Tianjin—seem to contribute the most among foreign sources to SMA nitrate, even though the magnitude and coverage of nitrate around BTH and COT are much greater. We believe this observed gap between concentrations at source regions and contributions at receptor regions bears important implications that highlight very critical characteristics of PM pollution in Northeast Asia. Namely, selective improvement of modeling inventories and sub-regional controls in upwind areas (e.g., China) may be necessary to avoid future high PM events in downwind areas (e.g., the SMA) like this episode. At the same time, we observe that the domestic contribution for nitrates is significant at the SMA; therefore, effective nitrate control for the SMA will require not only refined foreign control strategies accounting for geographically specific contributions but also appropriate domestic controls.

Relatively speaking, regional contributions of PM_{10} and $PM_{2.5}$ show similar patterns (Fig. 9). During the modeled period, relative contributions from each region change over time, with South Korea's domestic contribution tending to grow throughout the episode. For example, South Korean contribution to PM_{10} increased from 21% of 148 μg/m^3 on February 24–32% of 129 μg/m^3 on

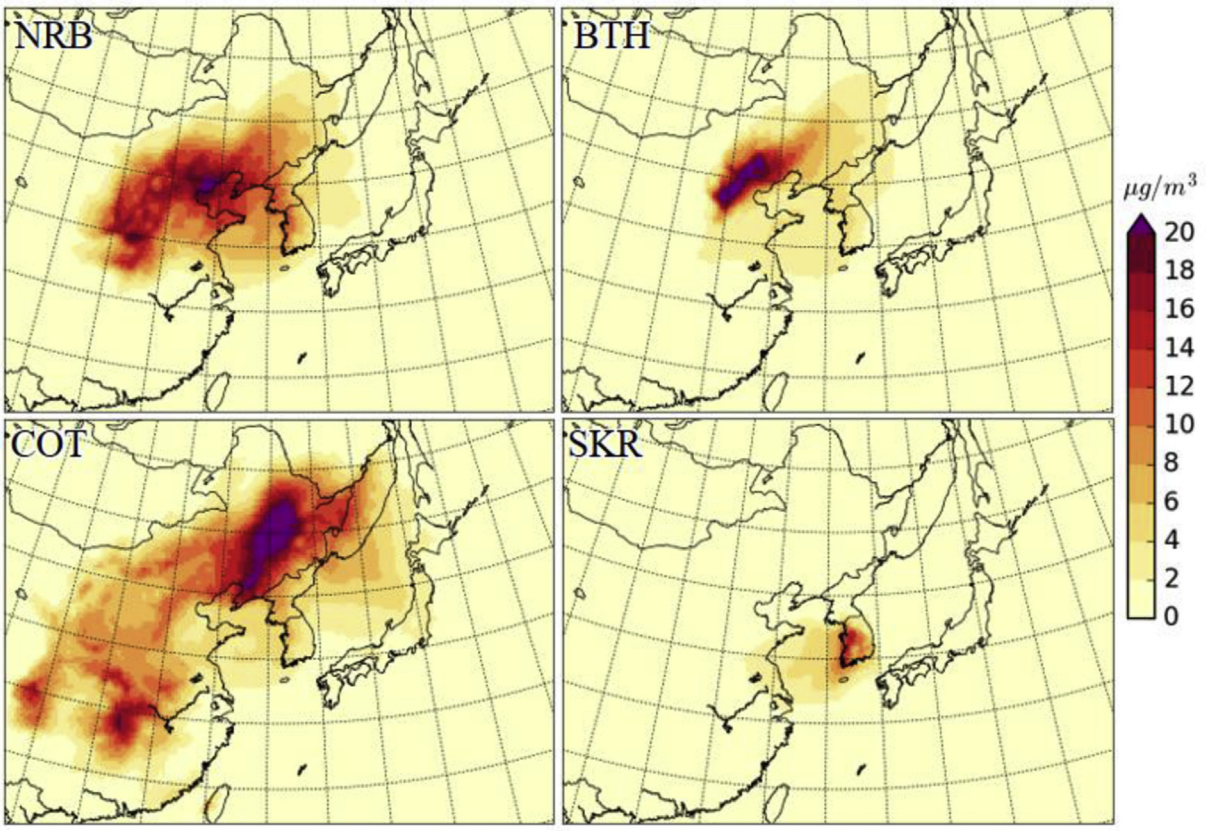

Fig. 8. Spatial distribution of episodic average (February 23 to 27, 2014) modeled contributions to nitrate concentrations for four major source regions.

February 26. At the same time, Chinese contributions were larger when higher-than-overall PM concentrations were modeled. On February 24, the highest PM_{10} day during the episode, Chinese contributions to PM_{10} reached 68%, while comprising 63% on February 26. Among Chinese regions, the NRB, BTH, and COT regions made major contributions to PM_{10} and $PM_{2.5}$ in the SMA.

For sulfate, the NRB, BTH, and COT regions dominated throughout the episode, with the magnitude of Chinese sulfate contribution rising until February 27. YRD contribution to sulfate become noticeable toward the end of episode. For nitrate, contributions by the NRB, BTH, and COT regions dominated during the early period of the episode, but South Korea's domestic contributions became the majority toward the end of the episode. NKR contributions were significant early in the episode but became insignificant later. For ammonium, South Korea was itself the major contributor throughout the episode. For organic matter, we observed a significant NKR contribution, comparable to the sum of all Chinese regions. Given that emissions from combustion processes are quite high in China, the possibility of under-estimated primary organic carbon emissions both in North Korea and China needs further investigation. At the same time, the ratio of elemental carbon to organic matter from South Korea seems to be lower than in other regions, suggesting that South Korea's domestic emissions characteristic also need review in the model.

For other $PM_{2.5}$, we noticed that CAMx has quite high bias in its prediction, with PSAT results indicating that the major portion was from China. Therefore, the possibility of gross over-estimation of other $PM_{2.5}$ emissions in China requires investigation. Due to relatively poor model performance in estimating organic matter and other $PM_{2.5}$ emissions, it is hard to draw definite, complete, and accurate conclusions about the contributions each region made for all PM species. Nevertheless, we believe that these PSAT results provide useful information to make quantitative source contribution assessments of some secondary inorganic aerosols (such as sulfate and nitrate), as well as to prioritize future directions for study.

After comparing observed and modeled total mass concentrations of PM_{10} and $PM_{2.5}$ during February 23 to 27, we found that CAMx agrees well with the episodic averaged PM_{10} mass concentrations in the SMA (Table 3). Comparison between model and observation at the BulGwang monitor indicates that CAMx might under-estimate certain portions of PM_{10} mass at that monitor and is also possibly missing some $PM_{2.5}$ mass concentrations. Observed and modeled $PM_{2.5}$ mass concentration over the modeled episode shows the same trend. Based on this study, we estimate that Chinese sources contributed 64% of PM_{10} and 70% of $PM_{2.5}$ mass concentrations in the SMA from February 23 to February 27, 2014. The greater relative Chinese contribution for $PM_{2.5}$ is most likely due to much higher local contributions of coarse PM in the SMA.

Combining model performance, the spatial distribution of regional contributions, and the species-by-species time series of contributions, we found an interesting characteristic in the analyzed period of February 23–27, 2014: high PM concentrations in the SMA were driven by sulfate from China, nitrate from China and South Korea, and ammonium from South Korea, although the balance of nitrate contributions from China and South Korea gradually shifted throughout the episode. During the wintertime, nitrate likely holds ammonium tightly, so ammonium will be balanced with available nitrate, with the rest of ammonium bound to either sulfate SO_4^{2-} or bisulfate HSO_4^- (NARSTO, 2004; Fountoukis and Nenes, 2007; Seinfeld and Pandis, 2016). We discuss the implications of this ion-balancing characteristic further in the

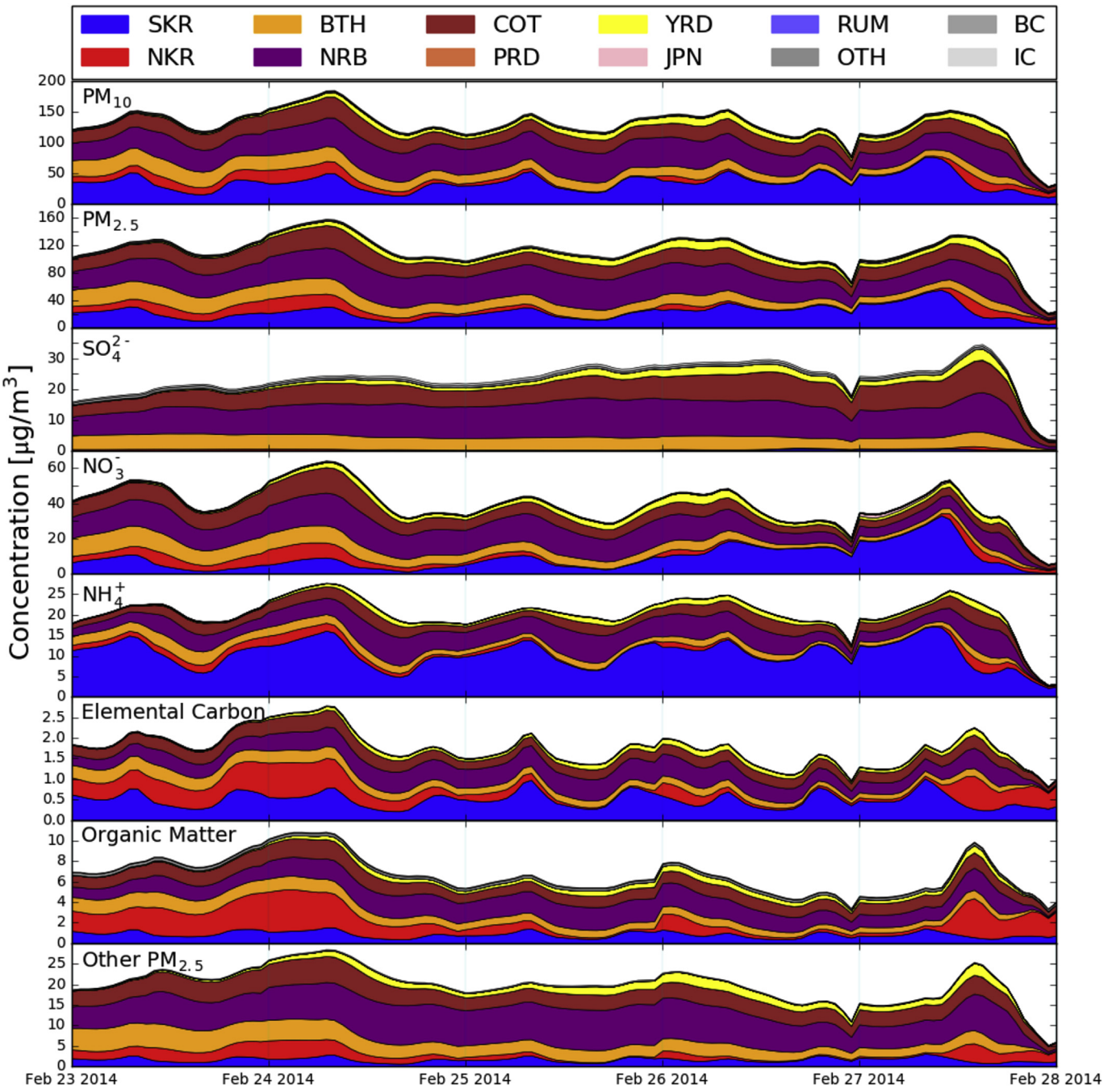

Fig. 9. Time series of modeled regional contributions to PM_{10}, $PM_{2.5}$, nitrate, sulfate, ammonium, elemental carbon, organic matter, and other $PM_{2.5}$ concentrations in the SMA, South Korea from February 23, 2014 to February 27, 2014.

following section.

With observation–model pairs for days showing higher-than-episodic average concentrations during the period from February 24 to February 27, 2014, we analyzed average observed and modeled concentrations of major $PM_{2.5}$ constituents in the SMA, South Korea. Overall, sulfate concentrations are underestimated and dominated by Chinese regions (Figs. 10 and 11). We speculate a possible cause for under-estimation: significant under-estimation of South Korea's domestic contribution and/or Chinese SO_2 emissions in the current inventory. By the same token, we observed that nitrate concentrations are over-estimated, with a significant South Korean contribution. As with sulfate, it is hard to conclude whether overestimation is due to over-estimated South Korean NO_X or Chinese nitrate. Interestingly, however, ammonium concentrations modeled by CAMx agree very well with observation.

Taking the agreement regarding total ammonium concentration between observation and model as a basis for further analysis, we may be able to backtrack region-specific sulfate and nitrate bound to ammonium, because cations and anions should be balanced in the atmosphere to reach thermodynamic equilibrium (Nenes et al., 1998; Fountoukis and Nenes, 2007; Pinder et al., 2008; Seinfeld and Pandis, 2016). For this further analysis, we applied the "degree of sulfate neutralization" (DSN) proposed by Pinder et al. (2008). DSN is defined as the ratio of molar ammonium concentration minus

Table 3
Average observed total mass and modeled total mass concentrations of PM_{10} and $PM_{2.5}$, along with estimated Chinese and domestic contributions to PM_{10} and $PM_{2.5}$, from February 23 to 27, 2014 in the SMA, South Korea.

	Observation (μg/m^3)	Model (μg/m^3)	Modeled Mass Contribution			Modeled Relative Contribution		
			China (μg/m^3)	South Korea (μg/m^3)	All Other Regions[a] (μg/m^3)	China (%)	South Korea (%)	All Other Regions[a] (%)
PM_{10}	138.4 (SMA average) 149.9 (at BulGwang Supersite)	131.8	84.3	36.5	11.0	64%	28%	8%
$PM_{2.5}$	121.9 (at BulGwang Supersite)	113.6	80.0	23.3	10.3	70%	21%	9%

[a] "All Other Regions" are all regions in the 27 km modeling domain excluding China and South Korea (i.e. Japan, North Korea, Russia, and Mongolia).

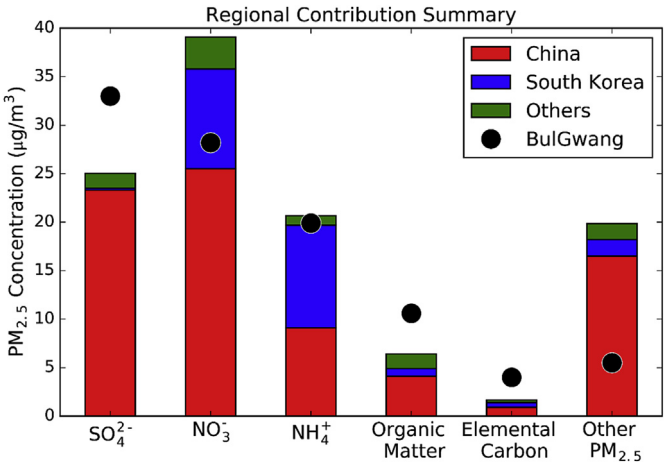

Fig. 10. Episodic average observed and modeled concentrations of major $PM_{2.5}$ constituents in the SMA, South Korea, from February 24 to February 27, 2014. Stacked bars show regional contributions estimated by modeling. Black circles indicate observed average concentrations of $PM_{2.5}$ constituents.

molar nitrate concentration to molar sulfate concentration (Pinder et al., 2008):

$$DSN = \frac{\frac{[NH_4^+]}{18} - \frac{[NO_3^-]}{62}}{\frac{[SO_4^{2-}]}{96}}$$

where $[NH_4^+]$, $[NO_3^-]$, and $[SO_4^{2-}]$ are mass concentrations in μg/m^3. DSN relies on the assumption that nitrate ion holds ammonium for full neutralization, while the rest of the ammonium binds with sulfate (or bisulfate) to neutralize fully (or partially). When DSN is 2, all ammonium sulfate ions are fully neutralized in the form of $(NH_4)_2SO_4$. If DSN is 1, all ammonium sulfate ions are in the form of ammonium bisulfate $(NH_4)HSO_4$. Overall, episodic average DSN in the SMA was observed as 1.89, while the modeled DSN is 2.0. The difference can be explained with two major issue. First, as we saw in the Fig. 6, the model underestimated SO_4^{2-} while overestimating NO_3^-. It is well-known that nitrates are often overestimated in photochemical modeling (Morris et al., 2005a; Tesche et al., 2006; Shimadera et al., 2016; Lu and Fung, 2016). Second, considering the above discussion of model performance, we think this DSN discrepancy is also likely due to some overage of ammonia or shortage of SO_2 in the model compared to reality.

To examine more closely, we can estimate a lumped DSN value for all Chinese regions aggregating ammonium, nitrate, and sulfate contributions by each Chinese source region while setting the total sulfate concentrations as the denominator. At the same time, because precursors from Chinese regions will likely react among themselves while Chinese precursors were still in China, we can assume that most of the ammonium from China, 9.1 μg/m^3 (=0.51 mol/m^3) bind with Chinese nitrate near source regions, which is 25.5 μg/m^3 (=0.41 mol/m^3) if we ignore that sulfuric acid has much stronger binding power with ammonium than nitric acid when ammonia is extremely limited. Then, only 0.094 mol/m^3 of Chinese ammonium are available to neutralize Chinese sulfate, which is 23.3 μg/m^3 (=0.24 mol/m^3). By taking the total sulfate ion concentrations, 25 μg/m^3 (=0.26 mol/m^3), we can estimate that Chinese DSN is 0.362 (=0.094/0.26) in the SMA. Superficially, this is puzzling; DSN of 0.362 suggests that only 36.2% of total sulfate ion molecules are neutralized, even in bisulfate form. However, some ammonium ions originate from other regions. For South Korea, we found that 0.41 mol/m^3 (=0.59 mol/m^3 of NH_4^+−0.17 mol/m^3 of NO_3^-−2 × 0.003 mol/m^3 of SO_4^{2-}) of ammonium ions are available after full neutralization of South Korean nitrate and sulfate. Like Chinese DSN, we could estimate the South Korea DSN as 1.6 (=0.41/0.26). These estimated DSN values are based on the following assumption: the respective region would have such a DSN value if precursors of like regions were more likely to neutralize then those from unlike regions. From Chinese and South Korean DSN values, we can infer that South Korea had ample ammonia available while China lacked ammonia to fully neutralize its nitrate and sulfate. In other words, most of the ammonium mass neutralizing Chinese secondary inorganic anion mass in the SMA must have been from South Korean ammonia emissions. Wang et al. (2016) reported similar findings in their annual simulations for 2010. This finding has significant implications, we believe, for the control mechanism of episodic secondary inorganic aerosol events, especially ammonium sulfates: secondary inorganic aerosols at the SMA during this event are a product of different major precursors originating from different regions. At the same time, we noticed significant temporal variations throughout the episode in ammonium, nitrate, and sulfate contributions by each region.

For nitrate, as shown in Figs. 9 and 11, South Korea's domestic contribution increased throughout the episode, while the Chinese contribution overall showed an opposite trend, except YRD. However, SKR consistently dominated the ammonium contribution. Sulfate contributions show various trends. BTH made relatively constant contributions for sulfate in the SMA. The most-contributing region, NRB, increased its contribution until its largest daily contribution, on February 25, with its sulfate contribution thereafter decreasing, although it remained the most-contributing region for sulfate on February 27. YRD and COT gradually increased their sulfate contributions.

For South Korea, the primary emission sources of NH_3 are area sources such as agricultural activities. During our analysis period, February 23–27, the total NH_3 emission was 2,978 tons and the area sources account for 81%. In terms of magnitude, the NH_3 emission in all countries in the 27 km domain except SKR is 212,617 tons. The NH_3 emissions from BTH, COT, and NRB are 16,392 tons, 117,265 tons, and 35,550 tons. Over 99% of these emissions are from area sources. Domination of area sources for NH_3 is very common in many places. If we calculate (moles of NH_3)/(moles of SO_2) in emissions, we can obtain 1.5 for the 27 km domain (excluding SKR),

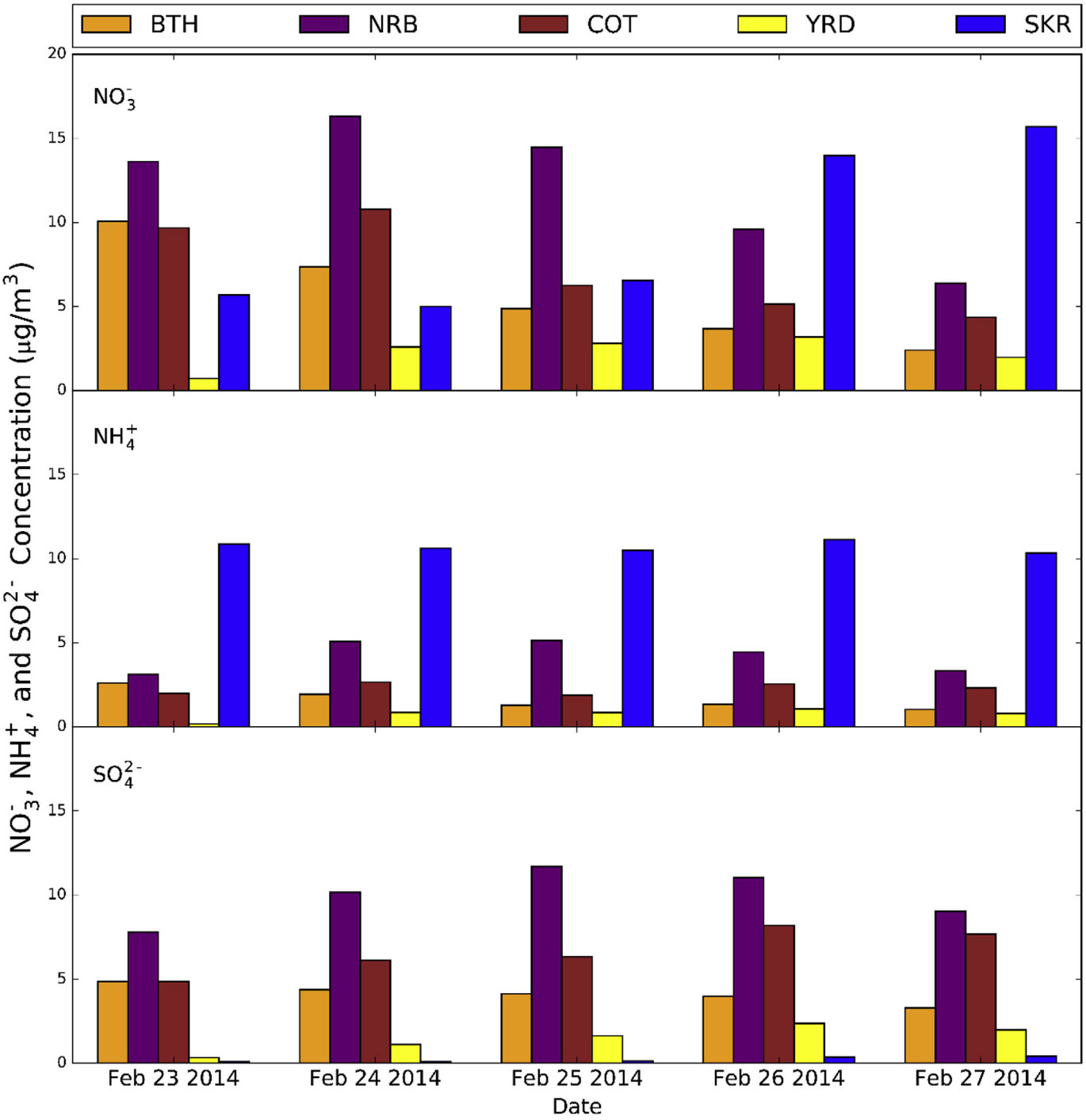

Fig. 11. Daily source contributions to nitrate (top), ammonium (middle), and sulfate (bottom) in the SMA, South Korea, from February 23 to February 27, 2014, from each source region.

1.3 for BTH, 1.6 for COT, 1.2 for NRB, and 2.0 for SKR, respectively. It indicates that excessive ammonia is likely available in SKR compared with Chinese regions, especially NRB and BTH. China has much stronger SO_2 sources (or weaker NH_3 sources) relatively compared with the emission condition in SKR. We recognize that this simple approach has a caveat; that is, it does not account for actual atmospheric chemical transformation that emitted precursors are undergoing.

To investigate region specific degree of neutralization during the transport, we could use regional specific molar concentrations for the DSN equation similar to what Wang et al. (2016) attempted to utilize. However, this approach will need much further validation because regional specific DNS assumes certain tendency of neutralization, e.g. Chinese ammonia neutralizing Chinese nitric acid, that is not necessarily true in all situations, especially at the downwind locations to assess the impact of upwind sources unless transport pattern is obvious as we discussed above. In fact, a proper examination on temporal evolution of region-specific neutralization requires a new kind of modeling tool that combines source-apportionment techniques and a history-tracking approach. It is

because we must follow the physicochemical history of air parcels originating from China until they arrive at the SMA to explain fully how secondary inorganic aerosols are formed and transported in the region.

4. Conclusion

Past studies of Northeast Asia have focused on either source-specific total PM contributions or chemical characteristics of downwind PM concentrations with low spatial resolution. Therefore, we conducted spatially and chemically resolved source-apportionment analyses using CAMx-PSAT, investigating the contributions of 10 source regions in Northeast Asia to PM_{10}, $PM_{2.5}$, and PM constituent concentrations in the SMA, South Korea, from February 22 to February 28, 2014. During the modeled episode, the SMA experienced high daily averaged PM_{10} concentrations (e.g., over 100 $\mu g/m^3$). We utilized an ensemble member of the IMAQS-K air quality forecasting system for South Korea using WRF for meteorology, emissions inputs comprising INTEX-B 2006, CAPSS 2007, and MEGAN for foreign anthropogenic, domestic anthropogenic, and biogenic emissions processed with SMOKE. We used a tagging-based source-apportionment tool, CAMx-PSAT, for chemical transport simulation in 27-km, 9-km, and 3-km two-way nested domains. The CAMx model performed reasonably well when compared to $PM_{2.5}$ measurements at USDOS monitors in China, PM_{10} measurements at NIER PM_{10} monitors in the SMA, and $PM_{2.5}$ measurements at the BulGwang Supersite. The case study period had observations of very high PM concentrations in areas near Beijing, with daily average PM_{10} and $PM_{2.5}$ concentrations over 200 $\mu g/m^3$ and 160 $\mu g/m^3$, respectively, from February 23 to February 27, 2014. Overall, Chinese contributions of PM_{10} and $PM_{2.5}$ mass concentrations in the SMA during the case study period were estimated at 64% and 70%, respectively.

From detailed source-apportionment analysis, we discovered critical characteristics of high PM events in the SMA. First, high PM events in the SMA are not only due to primary PM emissions from multiple sources but also because of complex chemical transformations of precursors originating from different sources. We observed that the high ammonium sulfate and ammonium nitrate concentrations in the SMA resulted from Chinese SO_2 and NO_X as well as South Korean NH_3 emissions. We believe this answers a question raised by Kim et al. (2006) regarding region-specific characteristics of secondary inorganic aerosol formation in South Korea. That is, a major portion of Chinese nitrate and sulfate were neutralized by South Korean ammonium, which also confirms what Wang et al. (2016) reported with their annual simulations for 2010. Second, the highest-PM regions in upwind areas (e.g., China) do not necessarily contribute the most to concentrations of certain PM species in downwind areas (e.g., South Korea), even if the highest-PM and most-contributing regions are close to one another. The model here suggests that, while BTH and COT regions seem to produce the highest nitrate concentrations in the region, NRB contributes the most nitrate to the SMA. This highlights the importance of fine-scale source apportionment and a careful review of region-by-region contributions. In addition, it also implies that meteorological features such as local and/or synoptic recirculation are important. Lastly, regional contributions were not constant but rather changed over time. For example, China was the major nitrate contributor in the early stage of the episode, while South Korea contributed much of the nitrates in the SMA at the end of the episode.

Based on our findings in this case study, we conclude that effective PM controls for the SMA will require appropriate domestic controls in addition to refined foreign control strategies that account for geographically specific contributions. In addition, future development of control strategy should consider the chemical characteristics of PM problems in upwind as well as downwind areas together by clarifying which regions need to reduce which primary PM species and/or precursor emissions. Further studies are warranted to temporally resolve quantitative contribution assessments at downwind areas while tracking the physicochemical history of air parcels originating from upwind areas to downwind ones.

Acknowledgements

This work was supported by the $PM_{2.5}$ Research Center established by the Ministry of Science, ICT, and Future Planning (MSIP) and the National Research Foundation (NRF) of Korea (grant number NRF-2014M3C8A5030624).

Appendix A. Supplementary data

Supplementary data related to this article can be found at http://dx.doi.org/10.1016/j.atmosenv.2017.05.006.

References

Bell, M.L., 2012. Assessment of the Health Impacts of Particulate Matter Characteristics (No. 161). Health Effects Institute, Boston, Massachusetts.

Burnett, R.T., Pope III, C.A., Ezzati, M., Olives, C., Lim, S.S., Mehta, S., Shin, H.H., Singh, G., Hubbell, B., Brauer, M., Anderson, H.R., Smith, K.R., Balmes, J.R., Bruce, N.G., Kan, H., Laden, F., Prüss-Ustün, A., Turner, M.C., Gapstur, S.M., Diver, W.R., Cohen, A., 2014. An Integrated Risk Function for Estimating the Global Burden of Disease Attributable to Ambient Fine Particulate Matter Exposure. Environmental Health Perspectives. http://dx.doi.org/10.1289/ehp.1307049.

Carter, W.P.L., 2016. SAPRC-99 Mechanism Files and Associated Programs and Examples [WWW Document]. http://www.engr.ucr.edu/~carter/SAPRC99/index.htm (Accessed November 13 2016).

Chang, J.S., Brost, R.A., Isaksen, I.S.A., Madronich, S., Middleton, P., Stockwell, W.R., Walcek, C.J., 1987. A three-dimensional Eulerian acid deposition model: physical concepts and formulation. J. Geophys. Res. 92, 14681–14700. http://dx.doi.org/10.1029/JD092iD12p14681.

Chang, L.-S., Cho, A., Park, H., Nam, K., Kim, D., Hong, J.-H., Song, C.-K., 2016. Human-model hybrid Korean air quality forecasting system. J. Air & Waste Manag. Assoc. 66, 896–911.

Chen, F., Dudhia, J., 2001. Coupling an advanced land surface–hydrology model with the penn state–NCAR MM5 modeling system. Part I: model implementation and sensitivity. Mon. Wea. Rev. 129, 569–585. http://dx.doi.org/10.1175/1520-0493(2001)129<0569:CAALSH>2.0.CO;2.

Chin, M., Diehl, T., Ginoux, P., Malm, W., 2007. Intercontinental transport of pollution and dust aerosols: implications for regional air quality. Atmos. Chem. Phys. 7, 5501–5517.

Colella, P., Woodward, P.R., 1984. The piecewise parabolic method (PPM) for gas-dynamical simulations. J. Comput. Phys. 54, 174–201.

Dentener, F., Keating, T., Akimoto, H., Pirrone, N., Dutchak, S., Zuber, A., 2010. Convention on long-range transboundary air pollution, United Nations, UNECE task force on emission inventories and projections. In: Hemispheric Transport of Air Pollution 2010: Prepared by the Task Force on Hemispheric Transport of Air Pollution Acting within the Framework of the Convention on Long-range Transboundary Air Pollution. Air pollution studies. United Nations, New York; Geneva.

Dominici, F., Greenstone, M., Sunstein, C.R., 2014. Particulate matter matters. Science 344, 257–259.

Eldred, R., 2003. Evaluation of the Equation for Soil Composite.

ENVIRON International Corporation, 2014. User's Guide: COMPREHENSIVE AIR QUALITY MODEL with EXTENSIONS Version 6.1.

Farrell, A., Keating, T., 1998. Multi-jurisdictional Air Pollution Assessment: a Comparison of the Eastern United States and Western Europe. Belfer Center for Science and International Affairs. Harvard University, Cambridge, MA.

Fountoukis, C., Nenes, A., 2007. ISORROPIA II: a computationally efficient thermodynamic equilibrium model for K^+–Ca^{2+}–Mg^{2+}–NH_4^+–Na^+–SO_4^{2-}–NO^{3-}–Cl^-–H_2O aerosols. Atmos. Chem. Phys. 7, 4639–4659.

Fu, X., Wang, S.X., Cheng, Z., Xing, J., Zhao, B., Wang, J.D., Hao, J.M., 2014. Source, transport and impacts of a heavy dust event in the Yangtze River Delta, China, in 2011. Atmos. Chem. Phys. 14, 1239–1254. http://dx.doi.org/10.5194/acp-14-1239-2014.

Gao, J., Tian, H., Cheng, K., Lu, L., Zheng, M., Wang, S., Hao, J., Wang, K., Hua, S., Zhu, C., others, 2015. The variation of chemical characteristics of $PM_{2.5}$ and PM_{10} and formation causes during two haze pollution events in urban Beijing, China. Atmos. Environ. 107, 1–8.

Guenther, C.C., 2006. Estimates of global terrestrial isoprene emissions using MEGAN (Model of Emissions of Gases and Aerosols from Nature). Atmos. Chem. Phys. 6.
Han, J.S., Moon, K.J., Ahn, J.Y., Hong, Y.D., Kim, Y.J., Ryu, S.Y., Cliff, S.S., Cahill, T.A., 2004. Characteristics of ion components and trace elements of fine particles at Gosan, Korea in spring time from 2001 to 2002. Environ. Monit. Assess. 92, 73–93.
Héroux, M.-E., Anderson, H.R., Atkinson, R., Brunekreef, B., Cohen, A., Forastiere, F., Hurley, F., Katsouyanni, K., Krewski, D., Krzyzanowski, M., others, 2015. Quantifying the health impacts of ambient air pollutants: recommendations of a WHO/Europe project. Int. J. public health 60, 619–627.
Hong, S.-Y., Dudhia, J., Chen, S.-H., 2004. A revised approach to ice microphysical processes for the bulk parameterization of clouds and precipitation. Mon. Wea. Rev. 132, 103–120. http://dx.doi.org/10.1175/1520-0493(2004)132<0103:ARATIM>2.0.CO;2.
Hong, S.-Y., Noh, Y., Dudhia, J., 2006. A new vertical diffusion package with an explicit treatment of entrainment processes. Mon. Wea. Rev. 134, 2318–2341. http://dx.doi.org/10.1175/MWR3199.1.
Jung, W., March 16, 2016. Environmental Challenges and Cooperation in Northeast Asia. Focus Asia, Institute for Security & Development Policy. No. 16. http://isdp.eu/publication/environmental-challenges-cooperation-northeast-asia (Accessed 17 September 2016).
Kain, J.S., 2014. The kain-fritsch convective parameterization: an update. J. Appl. Meteorol. 43, 170–181.
Kaiser, J., 1997. Showdown over clean air science. Science 277, 466–469.
Kim, H.C., Kim, S., Son, S.-W., Lee, P., Jin, C.-S., Kim, E., Kim, B.-U., Ngan, F., Bae, C., Song, C.-K., Stein, A., 2016a. Synoptic perspectives on pollutant transport patterns observed by satellites over East Asia: case studies with a conceptual model. Atmos. Chem. Phys. Discuss 1–30. http://dx.doi.org/10.5194/acp-2016-673.
Kim, J., Song, C., Ghim, Y., Won, J., Yoon, S., Carmichael, G., Woo, J., 2006. An investigation on NH_3 emissions and particulate NH_4^+–NO_3^- formation in East Asia. Atmos. Environ. 40, 2139–2150. http://dx.doi.org/10.1016/j.atmosenv.2005.11.048.
Kim, J.-H., Choi, D.-R., Koo, Y.-S., Lee, J.-B., Park, H.-J., 2016b. Analysis of domestic and foreign contributions using DDM in CMAQ during particulate matter episode period of february 2014 in Seoul. J. Korean Soc. Atmos. Environ. 32, 82–99. http://dx.doi.org/10.5572/KOSAE.2016.32.1.082.
Kim, O.-J., Ha, E.-H., Kim, B.-M., Seo, J.-H., Park, H.-S., Jung, W.-J., Lee, B.-E., Suh, Y.-J., Kim, Y.-J., Lee, J.-T., Kim, H., Hong, Y.-C., 2007. PM_{10} and pregnancy outcomes: a hospital-based cohort study of pregnant women in Seoul. J. Occup. Environ. Med. 49, 1394–1402. http://dx.doi.org/10.1097/JOM.0b013e3181594859.
Korea Meteorological Administration, 2016. Surface Observation [WWW Document]. http://web.kma.go.kr/eng/biz/observation_02.jsp.
Korea Ministry of Environment, 2016. Annual report of air quality in Korea 2015. Natl. Inst. Environ. Res. Incheon, South Korea.
Korea Ministry of Environment, 2015. Risk-oriented Air Quality Management [WWW Document]. http://eng.me.go.kr/eng/web/index.do?menuId=238 (Accessed September 17 2016).
Kwon, H.-J., Cho, S.-H., Chun, Y., Lagarde, F., Pershagen, G., 2002. Effects of the Asian dust events on daily mortality in Seoul, Korea. Environ. Res. 90, 1–5. http://dx.doi.org/10.1006/enrs.2002.4377.
Lee, D.-G., Lee, Y.-M., Jang, K.-W., Yoo, C., Kang, K.-H., Lee, J.-H., Jung, S.-W., Park, J.-M., Lee, S.-B., Han, J.-S., Hong, J.-H., Lee, S.-J., 2011. Korean national emissions inventory system and 2007 air pollutant emissions. Asian J. Atmos. Environ. 5, 278–291. http://dx.doi.org/10.5572/ajae.2011.5.4.278.
Liang, X., Li, S., Zhang, S., Huang, H., Chen, S.X., 2016. $PM_{2.5}$ data reliability, consistency, and air quality assessment in five Chinese cities. J. Geophys. Res. Atmos. http://dx.doi.org/10.1002/2016JD024877.
Lim, S.S., Vos, T., Flaxman, A.D., Danaei, G., Shibuya, K., Adair-Rohani, H., AlMazroa, M.A., Amann, M., Anderson, H.R., Andrews, K.G., others, 2012. A comparative risk assessment of burden of disease and injury attributable to 67 risk factors and risk factor clusters in 21 regions, 1990–2010: a systematic analysis for the Global Burden of Disease Study 2010. lancet 380, 2224–2260.
Lin, Y.-C., Hsu, S.-C., Chou, C.C.-K., Zhang, R., Wu, Y., Kao, S.-J., Luo, L., Huang, C.-H., Lin, S.-H., Huang, Y.-T., 2016. Wintertime haze deterioration in Beijing by industrial pollution deduced from trace metal fingerprints and enhanced health risk by heavy metals. Environ. Pollut. 208, 284–293. http://dx.doi.org/10.1016/j.envpol.2015.07.044.
Lipfert, F.W., 1994. Air Pollution and Community Health: a Critical Review and Data Sourcebook. John Wiley & Sons.
Lu, X., Fung, J., 2016. Source apportionment of sulfate and nitrate over the Pearl River Delta region in China. Atmosphere 7, 98. http://dx.doi.org/10.3390/atmos7080098.
Malm, W.C., Sisler, J.F., Huffman, D., Eldred, R.A., Cahill, T.A., 1994. Spatial and seasonal trends in particle concentration and optical extinction in the United States. J. Geophys. Res. Atmos. 99, 1347–1370.
Morris, R.E., Koo, B., Lau, S., Yarwood, G., 2005a. Application of CAMx and CMAQ Models to the August-september, 1997 SCOS Episode CRC Project a, pp. 40–42.
Morris, R.E., McNally, D.E., Tesche, T.W., Tonnesen, G., Boylan, J.W., Brewer, P., 2005b. Preliminary evaluation of the community Multiscale air quality model for 2002 over the Southeastern United States. J. Air & Waste Manag. Assoc. 55, 1694–1708. http://dx.doi.org/10.1080/10473289.2005.10464765.
NARSTO, 2004. Particulate Matter Science for Policy Makers: a NARSTO Assessment. Cambridge University Press, Cambridge, England.
National Institute of Environmental Research, 2013. Development of the Asia Emission Inventory in Support of Integrated Modeling of Climate and Air Quality (III) (No. NIER-SP2013–168).
Nenes, A., Pandis, S.N., Pilinis, C., 1998. ISORROPIA: a new thermodynamic equilibrium model for multiphase multicomponent inorganic aerosols. Aquat. Geochem. 4, 123–152. http://dx.doi.org/10.1023/A:1009604003981.
Nie, W., Wang, T., Xue, L.K., Ding, A.J., Wang, X.F., Gao, X.M., Xu, Z., Yu, Y.C., Yuan, C., Zhou, Z.S., Gao, R., Liu, X.H., Wang, Y., Fan, S.J., Poon, S., Zhang, Q.Z., Wang, W.X., 2012. Asian dust storm observed at a rural mountain site in southern China: chemical evolution and heterogeneous photochemistry. Atmos. Chem. Phys. 12, 11985–11995. http://dx.doi.org/10.5194/acp-12-11985-2012.
Oh, H.-R., Ho, C.-H., Kim, J., Chen, D., Lee, S., Choi, Y.-S., Chang, L.-S., Song, C.-K., 2015. Long-range transport of air pollutants originating in China: a possible major cause of multi-day high-PM_{10} episodes during cold season in Seoul, Korea. Atmos. Environ. 109, 23–30. http://dx.doi.org/10.1016/j.atmosenv.2015.03.005.
Pinder, R.W., Dennis, R.L., Bhave, P.V., 2008. Observable indicators of the sensitivity of $PM_{2.5}$ nitrate to emission reductions—Part I: derivation of the adjusted gas ratio and applicability at regulatory-relevant time scales. Atmos. Environ. 42, 1275–1286. http://dx.doi.org/10.1016/j.atmosenv.2007.10.039.
Pope, C.A., Dockery, D.W., 2006. Health effects of fine particulate air pollution: lines that connect. J. Air & Waste Manag. Assoc. 56, 709–742. http://dx.doi.org/10.1080/10473289.2006.10464485.
Qu, Y., An, J., He, Y., Zheng, J., 2016. An overview of emissions of SO_2 and NOx and the long-range transport of oxidized sulfur and nitrogen pollutants in East Asia. J. Environ. Sci. 44, 13–25. http://dx.doi.org/10.1016/j.jes.2015.08.028.
Ramboll-Environ, 2016. Comprehensive Air Quality Model with Extensions [WWW Document]. http://www.camx.com/ (Accessed September 20 2016).
Richey, M., Ohn, D., 2016. Pay the polluter: why South Korea and Japan should fund Abatement in China. Glob. Gov. A Rev. Multilater. Int. Organ. 22, 321–330.
Secretariat of Working Group for LTP project, 2011. Annual Report: the 11th Year's Joint Research on Long-range Transboundary Air Pollutants in Northeast Asia (No. Government Publication Registration Number: 11-1480083-000286-10).
Seinfeld, J.H., Carmichael, G.R., Arimoto, R., Conant, W.C., Brechtel, F.J., Bates, T.S., Cahill, T.A., Clarke, A.D., Doherty, S.J., Flatau, P.J., Huebert, B.J., Kim, J., Markowicz, K.M., Quinn, P.K., Russell, L.M., Russell, P.B., Shimizu, A., Shinozuka, Y., Song, C.H., Tang, Y., Uno, I., Vogelmann, A.M., Weber, R.J., Woo, J.-H., Zhang, X.Y., 2004. ACE-ASIA: regional climatic and atmospheric chemical effects of Asian dust and pollution. Bull. Am. Meteorol. Soc. 85, 367–380. http://dx.doi.org/10.1175/BAMS-85-3-367.
Seinfeld, J.H., Pandis, S.N., 2016. Atmospheric Chemistry and Physics: from Air Pollution to Climate Change. John Wiley & Sons.
Shimadera, H., Kojima, T., Kondo, A., 2016. Evaluation of air quality model performance for simulating long-range transport and local pollution of $PM_{2.5}$ in Japan. Adv. Meteorol. 2016, 1–13. http://dx.doi.org/10.1155/2016/5694251.
Shin, H.J., Park, S.-M., Park, J.S., Song, I.H., Hong, Y.D., 2016. Chemical characteristics of high PM episodes occurring in spring 2014, Seoul, Korea. Adv. Meteorol. 2016, 1–11. http://dx.doi.org/10.1155/2016/2424875.
Skamarock, W.C., Klemp, J.B., 2008. A time-split nonhydrostatic atmospheric model for weather research and forecasting applications. J. Comput. Phys. 227, 3465–3485. http://dx.doi.org/10.1016/j.jcp.2007.01.037.
Stein, A.F., Draxler, R.R., Rolph, G.D., Stunder, B.J.B., Cohen, M.D., Ngan, F., 2015. NOAA's HYSPLIT atmospheric transport and dispersion modeling system. Bull. Am. Meteorol. Soc. 96, 2059–2077. http://dx.doi.org/10.1175/BAMS-D-14-00110.1.
Stohl, A., Eckhardt, S., Forster, C., James, P., Spichtinger, N., 2002. On the pathways and timescales of intercontinental air pollution transport: INTERCONTINENTAL AIR POLLUTION TRANSPORT. J. Geophys. Res. Atmos. 107 http://dx.doi.org/10.1029/2001JD001396. ACH 6-1-ACH 6-17.
Strader, R., Lurmann, F., Pandis, S.N., 1999. Evaluation of secondary organic aerosol formation in winter. Atmos. Environ. 33, 4849–4863. http://dx.doi.org/10.1016/S1352-2310(99)00310-6.
Tan, J., Duan, J., He, K., Ma, Y., Duan, F., Chen, Y., Fu, J., 2009. Chemical characteristics of $PM_{2.5}$ during a typical haze episode in Guangzhou. J. Environ. Sci. 21, 774–781. http://dx.doi.org/10.1016/S1001-0742(08)62340-2.
Tesche, T.W., Morris, R., Tonnesen, G., McNally, D., Boylan, J., Brewer, P., 2006. CMAQ/CAMx annual 2002 performance evaluation over the eastern US. Atmos. Environ. Spec. issue Model Eval. Eval. Urban Reg. Eulerian Air Qual. model. 40, 4906–4919. http://dx.doi.org/10.1016/j.atmosenv.2005.08.046.
Uno, I., Satake, S., Carmichael, G.R., Tang, Y., Wang, Z., Takemura, T., Sugimoto, N., Shimizu, A., Murayama, T., Cahill, T.A., others, 2004. Numerical study of Asian dust transport during the springtime of 2001 simulated with the Chemical Weather Forecasting System (CFORS) model. J. Geophys. Res. Atmos. 109.
U.S. Department of State, 2016. Air Quality Monitoring Program [WWW Document]. http://www.stateair.net/web/historical/1/1.html (Accessed September 23 2016).
US EPA, 2009. Integrated Science Assessment for Particulate Matter (No. EPA/600/R-08/139F). RTP, NC.
Vedal, S., 1997. Ambient particles and health: lines that divide. J. Air & Waste Manag. Assoc. 47, 551–581.
Wagstrom, K.M., Pandis, S.N., Yarwood, G., Wilson, G.M., Morris, R.E., 2008. Development and application of a computationally efficient particulate matter apportionment algorithm in a three-dimensional chemical transport model. Atmos. Environ. 42, 5650–5659.
Wang, J., Xu, J., He, Y., Chen, Y., Meng, F., 2016. Long range transport of nitrate in the low atmosphere over Northeast Asia. Atmos. Environ. 144, 315–324. http://dx.doi.org/10.1016/j.atmosenv.2016.08.084.

Yan, R., Yu, S., Zhang, Q., Li, P., Wang, S., Chen, B., Liu, W., 2015. A heavy haze episode in Beijing in February of 2014: characteristics, origins and implications. Atmos. Pollut. Res. 6, 867–876. http://dx.doi.org/10.5094/APR.2015.096.

Yarwood, G., Morris, R.E., Wilson, G.M., 2007. Particulate matter source apportionment technology (PSAT) in the CAMx photochemical grid model. In: Air Pollution Modeling and its Application XVII. Springer, pp. 478–492.

Zhang, L., Brook, J.R., Vet, R., 2003. A revised parameterization for gaseous dry deposition in air-quality models. Atmos. Chem. Phys. 3, 2067–2082. http://dx.doi.org/10.5194/acp-3-2067-2003.

Zhang, L., Gong, S., Padro, J., Barrie, L., 2001. A size-segregated particle dry deposition scheme for an atmospheric aerosol module. Atmos. Environ. 35, 549–560. http://dx.doi.org/10.1016/S1352-2310(00)00326-5.

Zhang, Q., Streets, D.G., Carmichael, G.R., He, K.B., Huo, H., Kannari, A., Klimont, Z., Park, I.S., Reddy, S., Fu, J.S., others, 2009. Asian emissions in 2006 for the NASA INTEX-B mission. Atmos. Chem. Phys. 9, 5131–5153.